


RESEARCH

Open Access



Whole brain 3D MR fingerprinting in multiple sclerosis: a pilot study

Thomaz R. Mostardeiro^{1*} , Ananya Panda¹, Norbert G. Campeau¹, Robert J. Witte¹, Nicholas B. Larson², Yi Sui¹, Aiming Lu¹ and Kiaran P. McGee¹

Abstract

Background: MR fingerprinting (MRF) is a novel imaging method proposed for the diagnosis of Multiple Sclerosis (MS). This study aims to determine if MR Fingerprinting (MRF) relaxometry can differentiate frontal normal appearing white matter (F-NAWM) and splenium in patients diagnosed with MS as compared to controls and to characterize the relaxometry of demyelinating plaques relative to the time of diagnosis.

Methods: Three-dimensional (3D) MRF data were acquired on a 3.0T MRI system resulting in isotropic voxels ($1 \times 1 \times 1 \text{ mm}^3$) and a total acquisition time of 4 min 38 s. Data were collected on 18 subjects paired with 18 controls. Regions of interest were drawn over MRF-derived T_1 relaxometry maps encompassing selected MS lesions, F-NAWM and splenium. T_1 and T_2 relaxometry features from those segmented areas were used to classify MS lesions from F-NAWM and splenium with T-distributed stochastic neighbor embedding algorithms. Partial least squares discriminant analysis was performed to discriminate NAWM and Splenium in MS compared with controls.

Results: Mean out-of-fold machine learning prediction accuracy for discriminant results between MS patients and controls for F-NAWM was 65 % ($p = 0.21$) and approached 90 % ($p < 0.01$) for the splenium. There was significant positive correlation between time since diagnosis and MS lesions mean T_2 ($p = 0.015$), minimum T_1 ($p = 0.03$) and negative correlation with splenium uniformity ($p = 0.04$). Perfect discrimination ($AUC = 1$) was achieved between selected features from MS lesions and F-NAWM.

Conclusions: 3D-MRF has the ability to differentiate between MS and controls based on relaxometry properties from the F-NAWM and splenium. Whole brain coverage allows the assessment of quantitative properties within lesions that provide chronological assessment of the time from MS diagnosis.

Keywords: MR Fingerprinting, Multiple Sclerosis, Relaxometry, Normal appearing white matter, Splenium

Introduction

Multiple Sclerosis (MS) involves a wide spectrum of neurological symptoms resulting in challenging clinical management based on symptomatology alone [1]. Magnetic Resonance Imaging (MRI) has emerged as a powerful tool in the assessment of MS [2] with the requirement

that imaging is performed using standardized imaging protocols [3].

With high diagnostic sensitivity, conventional MRI is able to describe disease dissemination in time and space [4], classify MS subtypes [2] and evaluate treatment response [2, 5]. However, conventional MRI may be limited when distinguishing ongoing inflammatory demyelinating pathology in normal-appearing white matter

*Correspondence: Thomaz.r.mostardeiro@gmail.com

¹ Department of Radiology, Mayo Clinic, 200 1st St SW, Rochester, MN, USA

Full list of author information is available at the end of the article



despite known disease processes [6] as well as functional disability [7].

It has previously been demonstrated that MS pathology can be described through quantitative spatial mapping of MRI-derived relaxometry parameters, such as longitudinal (T_1) and transverse (T_2) relaxation times or proton density (PD) [8]. Further, parametric mapping may overcome the aforementioned limitations associated with MS diagnosis and staging by improving diagnostic accuracy [6, 9, 10] and predicting patient functional impairment [11, 12].

MRF is a novel MRI technique that allows quantitative mapping of T_1 , T_2 and PD using acquisition schemes followed by matching of the data to synthetically generated signals. The details of MRF have been described previously [13] and involve the repeated acquisition of image data over a time course in which acquisition parameters such as the flip angle, pulse repetition rate (TR) and echo time (TE) are intentionally modified [13]. Because the resultant time evolution of the signal in a given voxel is unique for a certain combination of tissue MR properties such as PD, T_1 and T_2 , MRF derived estimates of these parameters are generated by comparing the signal evolution history of a given voxel to a dictionary of pre-simulated signal evolutions [14].

Acquiring brain relaxometry values in clinically feasible times in patients with MS have been proposed with the QRAP-MASTER pulse sequence [15]. This technique has yet to meet the requirement of being obtainable within a relatively short acquisition time and as a result has had limited application as part of a standard, time constrained clinical MR examination. MRF has the potential to address this time constrain and has been described as a promising classifier of MS subtypes [16] within imaging times of several minutes. However, in that work the acquisition involved only 2D data and did not provide full brain coverage, limiting the clinical use of such an approach.

The purpose of this study is to determine if MR relaxometry maps derived from a fast 3D-MRF executed as part of a standard clinical MR examination sequence can differentiate frontal lobe normal appearing white matter (F-NAWM) and splenium in patients with MS versus healthy volunteers based solely on MRF-based relaxometry differences. Further, we hypothesize that MRF can detect MS lesions and establish a temporal relationship between relaxometry values and the time since diagnosis.

Materials and methods

Image acquisition and reconstruction

All clinical data were acquired on two 3T MR scanners (Discovery MR750 and Discovery MR750W,

GE Healthcare, Waukesha, WI) using an eight channel receive-only RF head coil. MRF data acquisition was performed using a 3D steady state free precession (SSFP) sequence with a multi-axis spiral trajectory [17]. Adiabatic inversion pulses were used before each acquisition. The flip angle ramped schedule ranged from 0.778° to 70° . Sequence details can be found in [17–19]. The acquisition FOV was $25.6 \times 25.6 \times 25.6 \text{ cm}^3$ with 1mm isotropic voxel resolution. The total acquisition time for the whole brain volume was 4 min 38 s. The T_1 range for the dictionary was from 10 to 3000 ms and T_2 from 10 ms to 2000 ms. Fingerprint reconstruction and dictionary matching were performed offline using Matlab (Mathworks, Natick, Massachusetts) on a 64bit Linux workstation equipped with two 8-core Intel Xeon Gold 6244 CPU @ 3.60 GHz, 376 GB system memory, and NVIDIA Tesla V100 GPU. The reconstruction pipeline has been described elsewhere [20].

Patient population

An Institutional Review Board (IRB) approved protocol was used to obtain MRF data in patients scheduled for a clinical MR exam. Informed consent was obtained by all the participants. All methods were carried out in accordance with institutional guidelines and regulations. The MRF sequence was acquired during the clinical MRI prior to the administration of a gadolinium-based contrast agent. A total of 18 subjects with an established diagnosis of MS were included: 14 subjects had relapsing remitting MS, 3 had secondary progressive MS and 1 had primary progressive MS. Three subjects had active gadolinium enhancing MS lesions. In the control group, 18 subjects were selected and paired to age and gender for each individual with MS. Twelve of the 18 MS patients (mean age of 49 ± 13 years (mean \pm SD)) were female. In the control group ($n = 18$; age mean \pm SD age: 49 ± 14), 12 patients were female.

Time-since-diagnosis was defined as the time between the MRF exam and the earliest medical record clearly stating in the medical impression the patient had MS. To allow a better assessment of normal appearing white matter changes in MS, a wide range of distribution for time-since-diagnosis of MS was included. Out of the 18 subjects, 5 had been diagnosed with MS in less than 6 months. The time-since-diagnosis ranged from 1 to 270 months. The median time-since-diagnosis was 69 months (Percentile 25: 10 months; Percentile 75: 113 months). The mean \pm SD time-since-diagnosis was 83 ± 79 months. The disease activity period (time since MS symptoms onset) largely corresponded to the time-since-diagnosis, except for 4 subjects who had MS

disease activity months (range: 18–120 months) before the formal diagnosis.

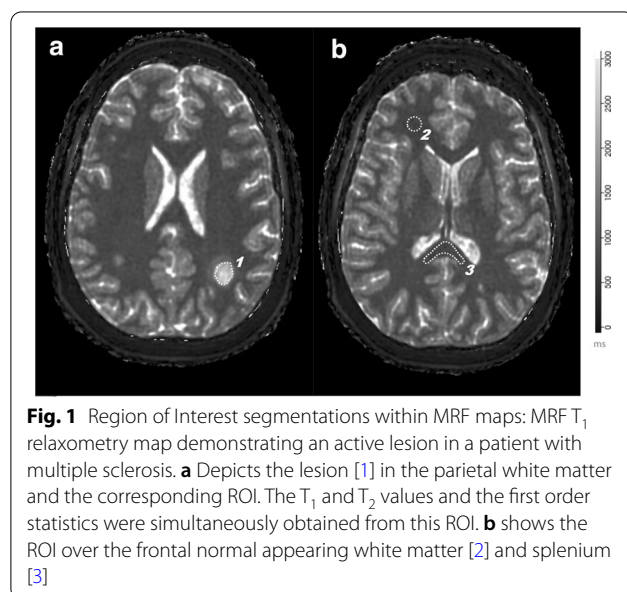
Regions of interest analysis

Segmentations were performed manually using 3D-Slicer software [20] as described in Fig. 1. Four to ten lesions were selected for each patient with MS, with a total of 105 lesions across 18 patients, 10 of which were active lesions. Perilesional edema was not included in the segmentation of active lesions. Additionally, for each patient, one ROI each in F-NAWM and splenium of the corpus callosum were drawn. F-NAWM was defined as areas without signal changes on the standard T2 weighted images in the clinical exam. In the control group, corresponding ROIs were drawn in the F-NAWM and splenium. First order statistics (interquartile range, skewness, uniformity, median, energy, robust mean absolute deviation, mean absolute deviation, total energy, maximum, root mean squared, 90 percentile, minimum, entropy, range, variance, 10 percentile, kurtosis, mean) obtained from each ROI were analyzed. All segmentations were reviewed by a Board certified neuroradiologist.

Statistical analysis

Distributional characteristics of categorical variables were summarized as counts and percentages, while quantitative values were summarized by means and standard deviations (SD) or medians and quartiles where indicated. Given the paired nature of the study design, univariate statistical comparisons between cases and controls were made for all individual relaxometry features (interquartile range, skewness, uniformity, median,

energy, robust mean absolute deviation, mean absolute deviation, total energy, maximum, root mean squared, 90 percentile, minimum, entropy, range, variance, 10 percentile, kurtosis, mean) using two-sided non-parametric Wilcoxon signed-rank tests. Visualization of multivariate relaxometry data was performed using unsupervised t-distributed stochastic neighbor embedding (t-SNE) dimensionality reduction based on two components under default settings. These visualizations were performed separately by T_1 and T_2 feature set as well as combined. Multivariate discrimination analysis between cases and controls for F-NAWM and splenium ROIs was performed using a two-component multi-level sparse partial least squares discriminant analysis (sPLS-DA) as implemented in the mixOmics R package [21]. These supervised machine learning analyses used a combined feature set from T_1 and T_2 relaxometry. Discrimination performance was characterized using area under the receiver operating characteristic curve (AUC) based on leave-one-out cross-validation along with corresponding p-values based on Wilcoxon testing. Univariate discrimination of MS lesions from F-NAWM and splenium using first order statistics features of centrality (mean and median) was evaluated using clustered ROC analyses to account for intra-patient correlation. Patient-level correlation testing between T_1 and T_2 relaxometry values and time since diagnosis for MS cases was performed using the nonparametric Kendall's tau rank correlation test, using the mean value across lesions for a given patient. Primary analyses focused on T_1 and T_2 lesion means, with exploratory analyses expanded out to all regions and feature types. All analyses were performed using the statistical software R v3.6.2, and all reported p-values are unadjusted for multiple testing.



Results

A representative MRF-based T_1 map paired with conventional weighted imaging is shown in Fig. 2.

Partial least squares discriminant analysis (PLS-DA) for F-NAWM and splenium is displayed in Fig. 3. Repeated cross validation ($n=5$) showed mean out-of-fold accuracy = 65% (AUC = 0.625 ($p=0.21$)) for discriminant results between patients and controls for F-NAWM, but mean out-of-fold accuracy approaching 90% (AUC = 0.880, $p < 0.0001$) for splenium, primarily via component 1. Examination of the component 1 feature loadings indicated maximum T_1 value (-0.30) and T_1 robust mean absolute deviation (-0.28). This was commensurate with univariate findings, where the top associations (Table 1) corresponded to T_1 distributional measures of extrema (e.g., T_1 90% percentile: Wilcoxon $p=0.002$) and variability (e.g., T_1 Root Mean Squared: Wilcoxon $p=0.003$).

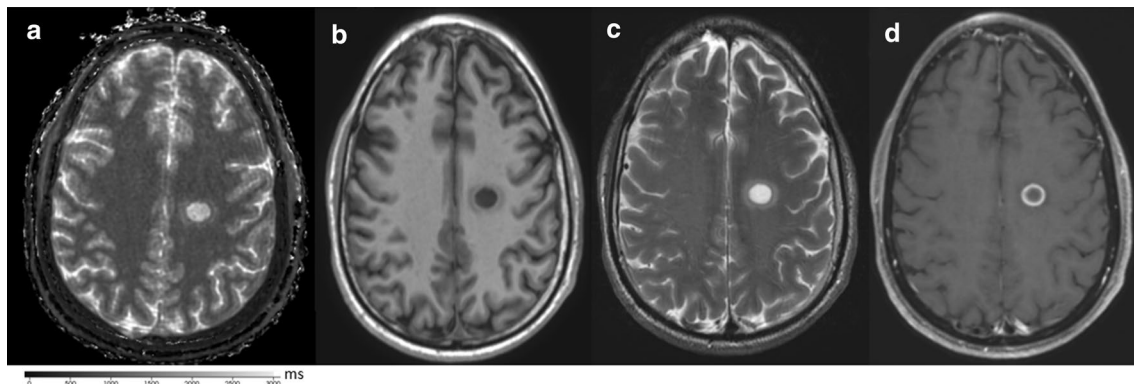


Fig. 2 Active lesion with surrounding edema in a patient confirmed with multiple sclerosis: **a** depicts the lesion in the parietal white matter on MRF-based T₁ map; **b** shows the same lesion in the same clinical exam in a T₁ weighted sequence, **c** illustrates the typical high intensity on a T₂ weighted spin echo sequence, and **d** confirms peripheral enhancement after gadolinium injection in a T₁ weighted sequence.

Table 1 Most significant individual relaxometry features allowing differentiation between splenium and frontal normal appearing white matter in multiple sclerosis

Relaxometry	Region	Feature	p value
T1	Splenium	90 percentile	0.002*
T1	Splenium	Root mean squared	0.003*
T1	Splenium	Mean	0.003*
T1	Splenium	Robust mean absolute deviation	0.005*
T1	Splenium	Median	0.005*
T1	Splenium	Interquartile range	0.006*
T1	Splenium	Mean absolute deviation	0.007*
T1	Splenium	Entropy	0.010*
T1	Splenium	Uniformity	0.012*
T2	Splenium	90 percentile	0.022*

*p < 0.05 connotes statistical significant. Two-sided non-parametric Wilcoxon signed-rank tests

The T-SNE Plot for classification of MS lesions is displayed on Fig. 4. AUC analysis for selected features demonstrated that median and mean T₁ and T₂ allowed perfect discrimination (AUC = 1) between splenium and lesions for both T₁ and T₂. Also, discrimination from F-NAWM was excellent (AUC = 1) and (AUC = 0.98) using median and mean for T₁ and T₂, respectively. Figure 5 depicts the distribution range of mean T₁ and T₂ relaxometry ranges for all structures analyzed.

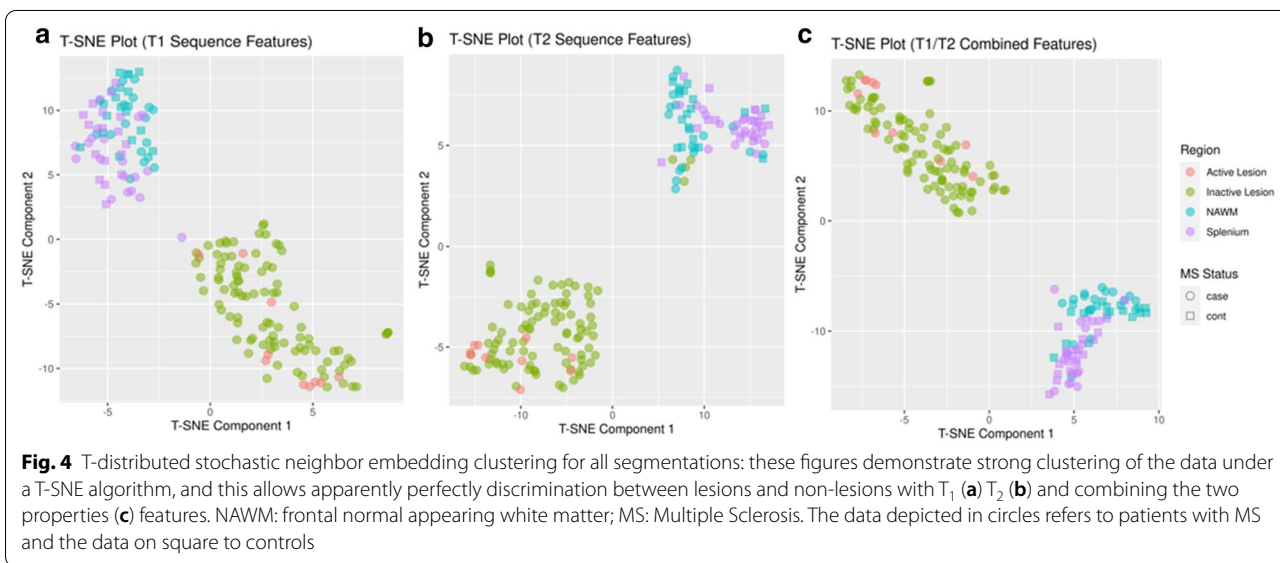
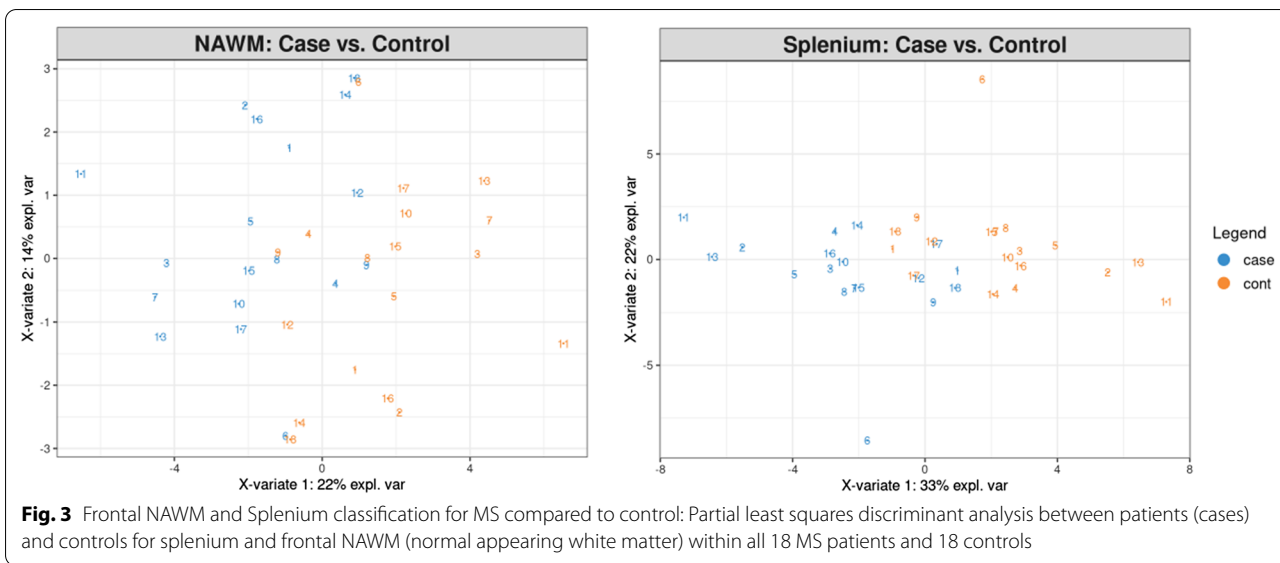
Correlation analyses among lesion means and time-since-diagnosis for MS cases was yielded higher rank correlation estimates for T₂ (rho = 0.419, p = 0.015) than T₁ (rho = 0.257, p = 0.11). The top five rank correlations among all relaxometry features and time since diagnosis are presented in Fig. 6.

Discussion

This work describes the use of a novel whole brain 3D MRF sequence [17, 18] in differentiating F-NAWM and splenium in patients with MS based on relaxometry estimates. Given the highly reproducible and accurate information provided by MR relaxometry [22, 23] the results of this study, and the isotropic whole brain coverage afforded by this technique, MRF has the potential for use in the diagnosis of patients with MS. The previously described application of MRF in the normal brain [22, 24], brain tumors [25, 26], epilepsy [27] and Parkinson disease [28], suggests that MRF has the potential for even broader application beyond MS.

MRI currently is a fundamental clinical tool when guiding therapy for patients with MS [29]. Given the complexity of the condition, several studies have been conducted with more advanced MRI techniques (such as myelin water fraction or functional MRI) to predict whether MS could be diagnosed by machine learning techniques [30–33]. Although the mentioned investigations have been successful, those techniques differ from MRF in that they do not provide a multi parametric approach from a single acquisition leading to lengthier exam acquisitions. Furthermore, the reproducibility of said techniques is not as well established as MRF-based relaxation estimates for both in vivo and phantom experiments [23, 34].

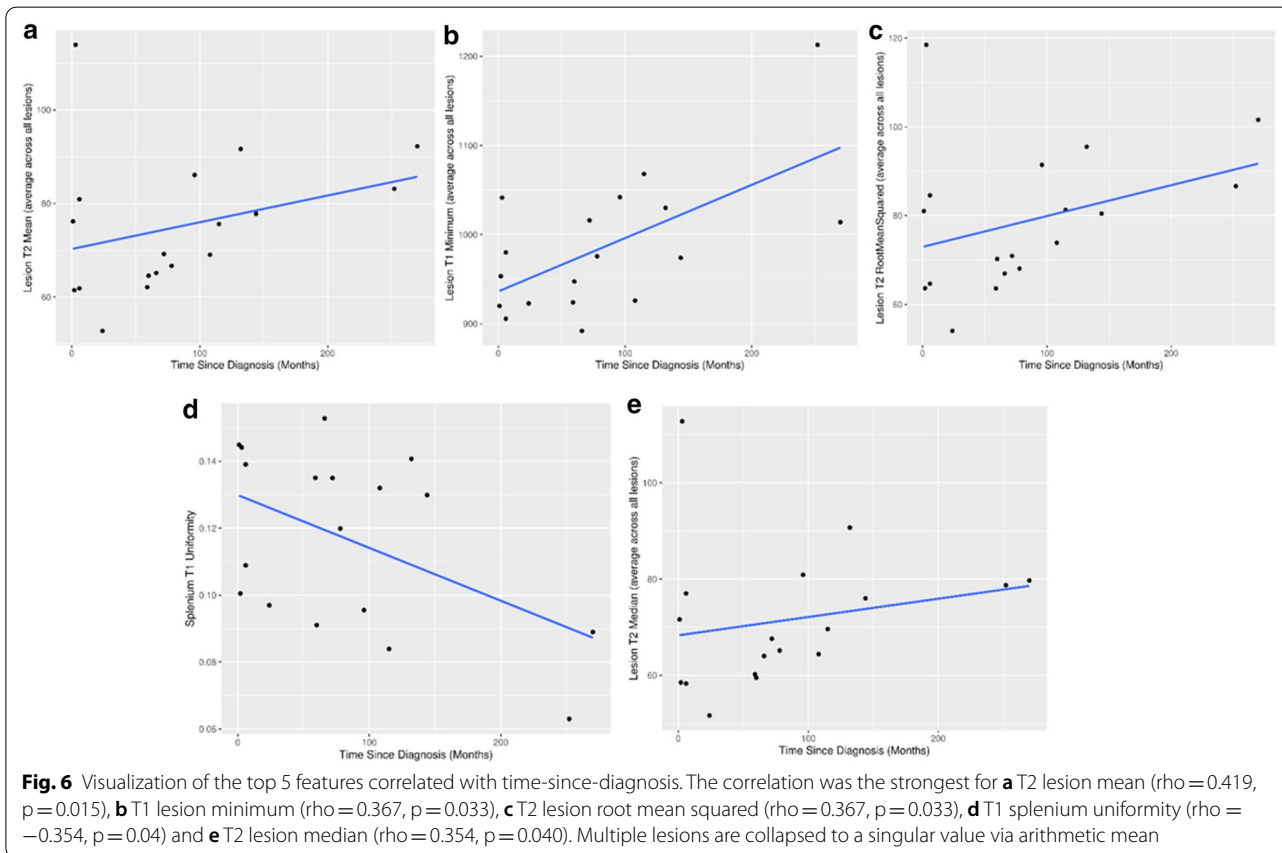
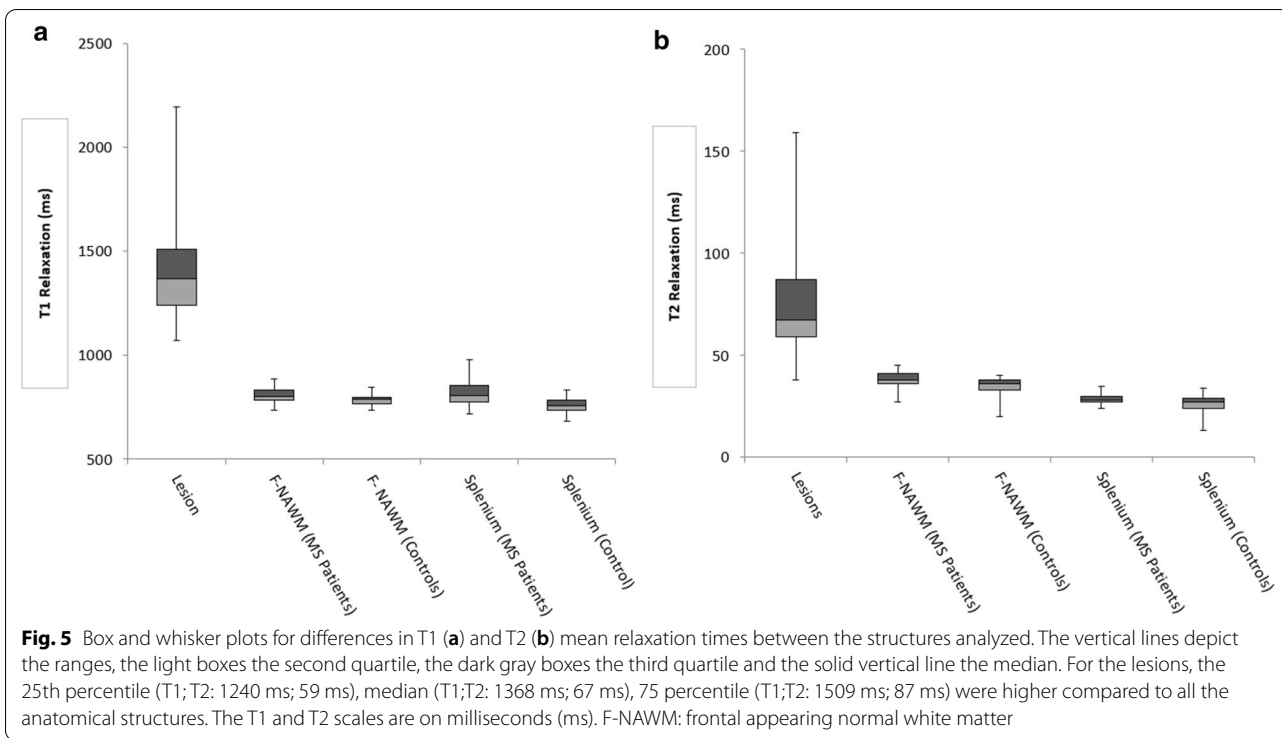
F-NAWM demonstrated longer relaxation in patients with MS in our study. This has been described by other quantitative imaging investigations [35]. Those changes are thought to be related with myelin histological changes in the white matter poorly defined by imaging [36] and importantly could predict clinical disability [12]. In this study, F-NAWM differentiation using MRF relaxation properties between cases and controls was fairly weak (mean out of fold accuracy = 65%). Given the moderate



sample size, it is possible larger samples could describe more robust differentiation. Also, it is important to note prior studies [35, 37, 38] have provided estimates of the entire NAWM through the brain, potentially including areas adjacent to MS plaques that can have subtle signal changes. In order to avoid this pitfall, values stated in this work were from segmented areas that only included white matter with no changes in the conventional T₂ weighted imaging and double inversion recovery.

Splenium is partially responsible for interhemispheric connections within the brain [39]. As such, studies describing splenium changes in patients with MS [40] have focused on diffusion tensor imaging. However,

histological changes in MS may also be responsible for relaxation lengthening in the splenium [35]. This could explain why ROI features related with a longer relaxation such as the percentile, mean and median were the most important in the differentiation of MS from controls in our study. The accuracy described in this study for classifying disease and control at this anatomical site based solely on MRF-based relaxometry changes was fairly strong (= 90%), identifying a major advantage of MRF. Given its potential to depict changes that are currently not seen or described in clinical practice, MRF may be useful, especially in those cases where the diagnosis of



MS is not clearly established by more conventional well-established imaging protocols.

It is known that time since diagnosis in MS can influence normal tissue relaxation [7, 11, 38], and that those changes could predict clinical disability [41, 42]. Papadoulos et al. [7] described NAWM relaxation changes in a longitudinal study covering 5 years. However, Davies et al. [11] found no significant differences in a three year longitudinal study after accessing T_1 quantitative changes through NAWM and GM. In this study, T_2 lengthening was observed in MS plaques on those patients with the longest time from diagnosis of MS to imaging. These findings could be related to a higher degree of Wallerian degeneration [43] although this finding has questionable clinical significance. Also, given this study was cross sectional, it would be valuable to investigate MRF through the same protocol in a longitudinal basis, so F-NAWM and splenium changes may be described and the faster acquisition as compared with the protocols mentioned [7, 41, 42] could be a valuable tool for clinical application. Importantly, this investigation described the diagnosis of MS as the surrogate for the disease duration. As such, given the onset of MS symptoms was before the time of the MS diagnosis for 4 volunteers (in a selected case by several years), the effects of disease activity before the diagnosis were not well described by our investigation.

This study has several limitations. The relatively small sample size may not be sufficient to effectively establish F-NAWM and splenium changes in MS as compared to controls. Also, F-NAWM segmentations represented a minimal fraction of the overall WM in all the patients included. Both active and non-active lesions were included, as defined by gadolinium enhancement in conventional T_1 weighted imaging, but given only 10 lesions were active, this study was not powered to detect changes within relaxometry for classifying lesion activity. Future studies with larger sample sizes and volumetric segmentation through normal appearing white matter may be considered.

Conclusions

3D-MRF relaxation changes in the splenium and to a lesser degree in the F-NAWM were able to discriminate the presence of MS disease as compared to controls. Those findings corroborate the potential clinical role of MRF relaxometry where suspicious white matter changes are present, as MRF could either support or counter the presumptive diagnosis. Furthermore, quantitative evaluation of MRF derived relaxometry was helpful in characterizing the chronicity of the demyelinating lesions.

Authors' contributions

All authors read and approved the final manuscript. TRM has made substantial contribution to the conception, design, acquisition, analysis, interpretation of data, drafted the work and substantively revised it. AP has made substantial contribution to the analysis, interpretation of data and substantively revised it. NGC has made substantial contribution to the analysis, interpretation of data and substantively revised it. RJW has made substantial contribution to the interpretation of data and substantively revised it. NBL has made substantial contribution analysis, interpretation of data and substantively revised it. YS has made substantial contribution to the conception, acquisition and substantively revised the work. AL has made substantial contribution to the conception and substantively revised it. KPM obtained institutional grant for this research and has made substantial contribution to the conception, design, acquisition, analysis, interpretation of data and substantively revised it.

Funding

This research was institutionally funded by the Mayo Clinic Center of Individualized Medicine at Rochester, Minnesota.

Availability of data and materials

The datasets used during the current study are available from the corresponding author on reasonable request.

Declarations

Ethics approval

This research was ethically approved by the Mayo Clinic Institutional Review Board (IRB number: 19-004479) and all participants were consented to participate in this research. All methods were carried out in accordance with institutional guidelines and regulations.

Consent for publication

Not applicable.

Competing interests

The authors declare that they have no competing interests.

Author details

¹Department of Radiology, Mayo Clinic, 200 1st St SW, Rochester, MN, USA.

²Department of Quantitative Health Sciences, Mayo Clinic, 200 1st St SW, Rochester, MN, USA.

Received: 6 January 2021 Accepted: 19 May 2021

Published online: 22 May 2021

References

1. Thompson AJ, Reingold SC, Cohen JA, International Panel on Diagnosis of Multiple S. Applying the 2017 McDonald diagnostic criteria for multiple sclerosis: authors' reply. *Lancet Neurol*. 2018;17(6):499–500.
2. Katz Sand I. Classification, diagnosis, and differential diagnosis of multiple sclerosis. *Curr Opin Neurol*. 2015;28(3):193–205.
3. Csepány T. [Diagnosis of multiple sclerosis: a review of the 2017 revisions of the McDonald criteria]. *Ideggyogy Sz*. 2018;71(9–10):321–9.
4. Brownlee WJ, Hardy TA, Fazekas F, Miller DH. Diagnosis of multiple sclerosis: progress and challenges. *Lancet*. 2017;389(10076):1336–46.
5. Dale RC, Pillai SC. Early relapse risk after a first CNS inflammatory demyelination episode: examining international consensus definitions. *Dev Med Child Neurol*. 2007;49(12):887–93.
6. Lommers E, Simon J, Reuter G, Delrue G, Dive D, Degueudre C, et al. Multiparameter MRI quantification of microstructural tissue alterations in multiple sclerosis. *Neuroimage Clin*. 2019;23:101879.
7. Papadopoulos K, Tozer DJ, Fisniku L, Altmann DR, Davies G, Rashid W, et al. T_1 -relaxation time changes over five years in relapsing-remitting multiple sclerosis. *Mult Scler*. 2010;16(4):427–33.
8. Zellini F, Niepel G, Tench CR, Constantinescu CS. Hypothalamic involvement assessed by T_1 relaxation time in patients with relapsing-remitting multiple sclerosis. *Mult Scler*. 2009;15(12):1442–9.

9. Krauss W, Gunnarsson M, Nilsson M, Thunberg P. Conventional and synthetic MRI in multiple sclerosis: a comparative study. *Eur Radiol*. 2018;28(4):1692–700.
10. Mainero C, Louapre C, Govindarajan ST, Gianni C, Nielsen AS, Cohen-Adad J, et al. A gradient in cortical pathology in multiple sclerosis by in vivo quantitative 7 T imaging. *Brain*. 2015;138(Pt 4):932–45.
11. Davies GR, Hadjiprocopis A, Altmann DR, Chard DT, Griffin CM, Rashid W, et al. Normal-appearing grey and white matter T1 abnormality in early relapsing-remitting multiple sclerosis: a longitudinal study. *Mult Scler*. 2007;13(2):169–77.
12. Manfredonia F, Ciccarelli O, Khaleeli Z, Tozer DJ, Sastre-Garriga J, Miller DH, et al. Normal-appearing brain t1 relaxation time predicts disability in early primary progressive multiple sclerosis. *Arch Neurol*. 2007;64(3):411–5.
13. Ma D, Gulani V, Seiberlich N, Liu K, Sunshine JL, Duerk JL, et al. Magnetic resonance fingerprinting. *Nature*. 2013;495(7440):187–92.
14. Kurzawski JW, Cencini M, Peretti L, Gomez PA, Schulte RF, Donatelli G, et al. Retrospective rigid motion correction of three-dimensional magnetic resonance fingerprinting of the human brain. *Magn Reson Med*. 2020;84(5):2606–15.
15. Krauss W, Gunnarsson M, Andersson T, Thunberg P. Accuracy and reproducibility of a quantitative magnetic resonance imaging method for concurrent measurements of tissue relaxation times and proton density. *Magn Reson Imaging*. 2015;33(5):584–91.
16. Nakamura K, Deshmone A, Guruprakash D, Jiang Y, Ma, D, Lee, J, et al. A Novel Method for Quantification of Normal Appearing Brain Tissue in Multiple Sclerosis: Magnetic Resonance Fingerprinting American Academy of Neurology Meeting; 04/05/2016; San Francisco 2016.
17. Cao X, Ye H, Liao C, Li Q, He H, Zhong J. Fast 3D brain MR fingerprinting based on multi-axis spiral projection trajectory. *Magn Reson Med*. 2019;82(1):289–301.
18. Buonincontri G, Kurzawski JW, Kaggie JD, Matys T, Gallagher FA, Cencini M, et al. Three dimensional MRF obtains highly repeatable and reproducible multi-parametric estimations in the healthy human brain at 1.5T and 3T. *Neuroimage*. 2021;226:117573.
19. Gomez PA, Cencini M, Golbabaee M, Schulte RF, Pirkl C, Horvath I, et al. Rapid three-dimensional multiparametric MRI with quantitative transient-state imaging. *Sci Rep*. 2020;10(1):13769.
20. Cruz G, Schneider T, Bruijnen T, Gaspar AS, Botnar RM, Prieto C. Accelerated magnetic resonance fingerprinting using soft-weighted key-hole (MRF-SOHO). *PLoS One*. 2018;13(8):e0201808.
21. Rohart F, Gautier B, Singh A, KA LC. mixOmics: An R package for omics feature selection and multiple data integration. *PLoS Comput Biol*. 2017;13(11):e1005752.
22. Buonincontri G, Biagi L, Retico A, Cecchi P, Cosottini M, Gallagher FA, et al. Multi-site repeatability and reproducibility of MR fingerprinting of the healthy brain at 1.5 and 3.0T. *Neuroimage*. 2019;195:362–72.
23. Korzdorfer G, Kirsch R, Liu K, Pfeuffer J, Hensel B, Jiang Y, et al. Reproducibility and repeatability of MR fingerprinting relaxometry in the human brain. *Radiology*. 2019;292(2):429–37.
24. Badve C, Yu A, Rogers M, Ma D, Liu Y, Schluchter M, et al. Simultaneous T1 and T2 brain relaxometry in asymptomatic volunteers using magnetic resonance fingerprinting. *Tomography*. 2015;1(2):136–44.
25. Badve C, Yu A, Dastmalchian S, Rogers M, Ma D, Jiang Y, et al. MR fingerprinting of adult brain tumors: initial experience. *AJNR Am J Neuroradiol*. 2017;38(3):492–9.
26. de Blank P, Badve C, Gold DR, Stearns D, Sunshine J, Dastmalchian S, et al. Magnetic resonance fingerprinting to characterize childhood and young adult brain tumors. *Pediatr Neurosurg*. 2019;54(5):310–8.
27. Wang K, Cao X, Wu D, Liao C, Zhang J, Ji C, et al. Magnetic resonance fingerprinting of temporal lobe white matter in mesial temporal lobe epilepsy. *Ann Clin Transl Neurol*. 2019;6(9):1639–46.
28. Keil VC, Bakoeva SP, Jurcoane A, Doneva M, Amthor T, Koken P, et al. A pilot study of magnetic resonance fingerprinting in Parkinson's disease. *NMR Biomed*. 2020;33(11):e4389.
29. Garcia Merino A, Blasco MR. Confirming the MS diagnosis. *Int MS J*. 2007;14(2):58–63.
30. Sacca V, Sarica A, Novellino F, Barone S, Tallarico T, Filippelli E, et al. Evaluation of machine learning algorithms performance for the prediction of early multiple sclerosis from resting-state fMRI connectivity data. *Brain Imaging Behav*. 2019;13(4):1103–14.
31. Neeb H, Schenk J, Weber B. Multicentre absolute myelin water content mapping: development of a whole brain atlas and application to low-grade multiple sclerosis. *Neuroimage Clin*. 2012;1(1):121–30.
32. Eitel F, Soehler E, Bellmann-Strobl J, Brandt AU, Rupprecht K, Giess RM, et al. Uncovering convolutional neural network decisions for diagnosing multiple sclerosis on conventional MRI using layer-wise relevance propagation. *Neuroimage Clin*. 2019;24:102003.
33. Yoo Y, Tang LYW, Brosch T, Li DKB, Kolind S, Vavasour I, et al. Deep learning of joint myelin and T1w MRI features in normal-appearing brain tissue to distinguish between multiple sclerosis patients and healthy controls. *Neuroimage Clin*. 2018;17:169–78.
34. Jiang Y, Ma D, Keenan KE, Stupic KF, Gulani V, Griswold MA. Repeatability of magnetic resonance fingerprinting T1 and T2 estimates assessed using the ISMRM/NIST MRI system phantom. *Magn Reson Med*. 2017;78(4):1452–7.
35. Neema M, Goldberg-Zimring D, Guss ZD, Healy BC, Guttmann CR, Houtchens MK, et al. 3 T MRI relaxometry detects T2 prolongation in the cerebral normal-appearing white matter in multiple sclerosis. *Neuroimage*. 2009;46(3):633–41.
36. Seewann A, Vrenken H, van der Valk P, Blezer EL, Knol DL, Castelijns JA, et al. Diffusely abnormal white matter in chronic multiple sclerosis: imaging and histopathologic analysis. *Arch Neurol*. 2009;66(5):601–9.
37. Gracien RM, Reitz SC, Hof SM, Fleischer V, Zimmermann H, Droby A, et al. Assessment of cortical damage in early multiple sclerosis with quantitative T2 relaxometry. *NMR Biomed*. 2016;29(4):444–50.
38. Steenwijk MD, Vrenken H, Jonkman LE, Daams M, Geurts JJ, Barkhof F, et al. High-resolution T1-relaxation time mapping displays subtle, clinically relevant, gray matter damage in long-standing multiple sclerosis. *Mult Scler*. 2016;22(10):1279–88.
39. Pagani E, Horsfield MA, Rocca MA, Filippi M. Assessing atrophy of the major white matter fiber bundles of the brain from diffusion tensor MRI data. *Magn Reson Med*. 2007;58(3):527–34.
40. Bodini B, Cercignani M, Khaleeli Z, Miller DH, Ron M, Penny S, et al. Corpus callosum damage predicts disability progression and cognitive dysfunction in primary-progressive MS after five years. *Hum Brain Mapp*. 2013;34(5):1163–72.
41. Gracien RM, Jurcoane A, Wagner M, Reitz SC, Mayer C, Volz S, et al. The relationship between gray matter quantitative MRI and disability in secondary progressive multiple sclerosis. *PLoS ONE*. 2016;11(8):e0161036.
42. Gracien RM, Jurcoane A, Wagner M, Reitz SC, Mayer C, Volz S, et al. Multimodal quantitative MRI assessment of cortical damage in relapsing-remitting multiple sclerosis. *J Magn Reson Imaging*. 2016;44(6):1600–7.
43. Seewann A, Kooi EJ, Roosendaal SD, Barkhof F, van der Valk P, Geurts JJ. Translating pathology in multiple sclerosis: the combination of postmortem imaging, histopathology and clinical findings. *Acta Neurol Scand*. 2009;119(6):349–55.

Publisher's Note

Springer Nature remains neutral with regard to jurisdictional claims in published maps and institutional affiliations.